A nonlinear elastic deformable template for soft structure segmentation. Application to the heart segmentation in MRI

Youssef Rouchdy[a], Jérôme Pousin[a], Joël Schaerer[b], Patrick Clarysse[b]

a: Institut C. Jordan, UMR CNRS 5028, Centre des Mathématiques, bat. L. De Vinci, INSA de Lyon, 69621 Villeurbanne cedex, France
b: CREATIS CNRS UMR 5515, INSERM U630 INSA Bât. Blaise Pascal, 69621 Villeurbanne cedex, France

Abstract. This article proposes a nonlinear 3D deformable model for the image segmentation of soft structure. The template is modeled as an elastic body which is deformed by forces derived from the image. It relies on a template, which is a topological, geometrical and material model of the structure to segment. This model is based on the nonlinear three-dimensional elasticity problem with a boundary condition of pure traction. In addition, the applied forces are successive, as they depend on the displacements. For computations, an incremental algorithm is proposed to minimize the global energy of template deformation. Sufficient conditions of the convegence for the incremental algorithm are given. Finally, a discrete algorithm using the finite element method is presented and evaluated on synthetic images and actual MR images of mice.

1. Introduction

Modern medical imaging systems can provide a great amount of data explaining the anatomy and function of the patient's organs. However, the development of efficient tools for automatic processing is mandatory to fully exploit the wealth of information obtained by medical imaging systems and to provide quantified parameters. The context of this paper is related to the extraction of the heart's anatomy and motion from temporal image sequences, more precisely Magnetic Resonance Imaging (MRI) sequences. Currently, a clinical examination results in a stack of slices covering the whole heart at successive time points over the cardiac cycle. Interpolation techniques can reconstruct 3D volumes at each time point. The reconstructed volumes constitute the input of the segmentation tracking approach proposed in this paper. Let's formalize the 3D imaging data. A volume data set is denoted by a matrix V with x rows, y column's and z slices which represents a discrete grid of volume elements (or voxels) $v \in \{1, \cdot\cdot, X\} \times \{1, \cdot\cdot, Y\} \times \{1, \cdot\cdot, Z\}$. For each voxel v, we denote the gray level function by $I : \mathbb{N}^3 \longrightarrow \mathcal{Z},\ v \mapsto I(v)$. The data are anisotropic with an equal sampling in the x and y directions but with a lower resolution along the z-direction. Image segmentation refers to the process which identifies all voxels that belong to the same structure according to a certain homogeneity criterion (most often this criterion is the gray level). Segmentation is required for the identification of the object (for instance the heart) in the MRI volume data. Here, we deal with edge-based algorithms which try to detect the border of a structure, that is to say the discontinuity surfaces of the gray level function I.

The methodology we follow for the segmentation is based on the deformable model principle and, as such, relies on *a priori* model of the structure to be segmented [19]. In the great variety of the deformable models, our approach uses a volumetric tetrahedral mesh of the heart with elastic properties. We call it Deformable Elastic Template (DET). The linear DET model has been previously introduced in [21]. In this paper, we introduce the nonlinear DET model which is able to take into account large displacements, a major limitation of the linear version.

The segmentation scheme proceeds in three stages [21]. Firstly, a reference mesh of a given anatomical structure is created. In the present case, a volumetric tetrahedral mesh of the heart including both left and right ventricles was extracted from a reference data set. The mesh size is a tradeoff between computation time and accuracy of shape representation. The quality of the mesh elements is controlled throughout the deformation by the estimation of a quality criterion defined in [2]. Secondly, the reference mesh is positioned into the image with in an iterative affine transform process until the minimization of a similarity measure between the reference model and the image data is achieved. The template is first scaled to correct dimensions, with respect to the image resolution, and translated so that a few number of reference points of the template and in the image matchs. We look a 3-D rigid transformation which brings the template as close as possible to the anatomical structures of interest.

The 3D rigid transformation results from the minimization of a combined edge and region energy term with an approach similar to the one presented in [22]. Figure 1 the automatic initial positionning of the template through a global affine transformation for a mid-ventricular slice of a heart patient. The left picture shows the initial position of the template and the right picture shows the registration result.

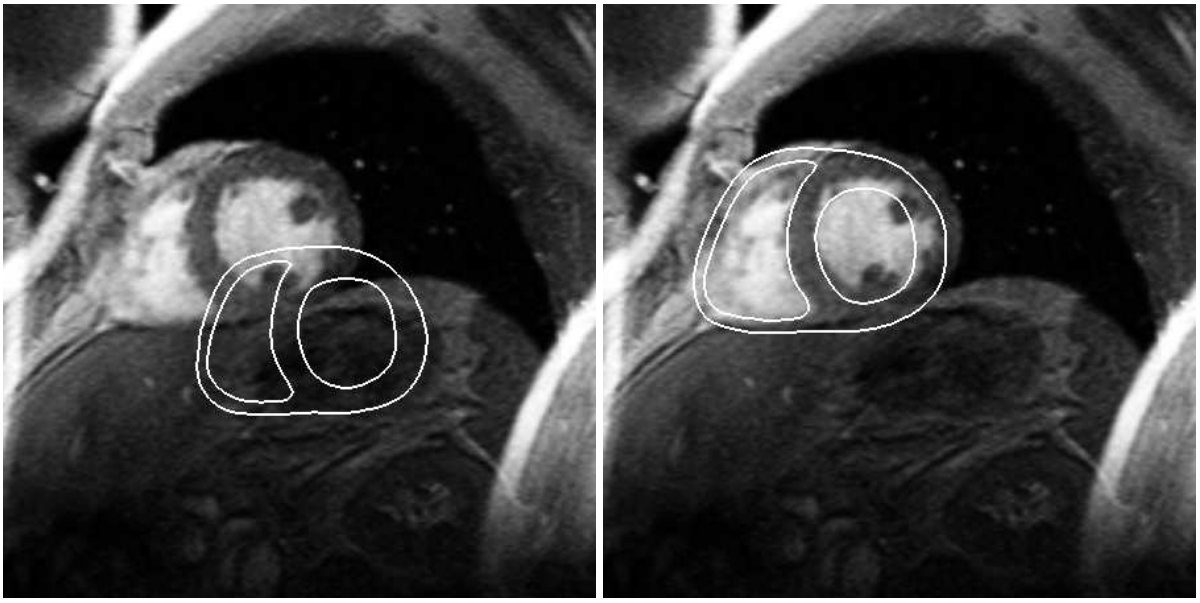

(a) (b)

Figure 1. (a): Trace of the reference template in a 2D MR slice before registration, (b): The reference template after affine registration

In the last stage, the model is locally adapted to fit the structure borders. This is achieved by minimizing a global energy which consists of an internal elasticity term and an external energy term which reflects the proximity to the target borders in the image.

This paper focuses on the last step of the segmentation, which involves nonlinear elasticity. An incremental method for the minimization of the global energy is proposed and its convergence properties are demonstrated. It is assumed that the minimization of the global energy is equivalent to solving Euler optimal conditions which corresponds in this case to a nonlinear elasticity boundary problem. A major difficulty in the numerical solution of large displacements and deformations of elastic structures is the proper handling of the various non-linearities that occur in the boundary value problems of elasticity. To deal with this difficulty, Ciarlet proposes in [7] an incremental method for pure displacements. The incremental method consists in letting the forces vary by small increments from 0 to the given ones and compute corresponding approximate solutions by successive linearization. In this work, the incremental method is adapted to image segmentation. The proposed algorithm is discretized with a finite element method and evaluated both on synthetic images and cardiac MR images.

2. Related work

Segmentation and motion estimation of the cardiac structures is one of the most popular applications in image analysis. Numerous segmentation techniques have been tested in this context from basic thresholding and low-level methods to more sophisticated modeling and learning approaches [11]. The used methodology and the results depend on the imaging modalities and the number of considered dimensions (2D, 3D, 2D+time, 3D+time). Up to now, Magnetic Resonance Imaging and Ultrasounds have been mainly addressed for both static and dynamic segmentation. However, the inherent difficulties (image artifacts, noise and motion) are such that no generic method has truly emerged yet for routine practice. It is clear that a priori knowledge needs to be taken into account to better constrain the segmentation. Therefore, methods based on a priori models of the heart geometry, known as deformable models, have retained attention and obtained a certain success in practice. As mentioned before, the final segmentation results from the minimization of a global energy functional which finds the balance between an internal energy, constraining the structure shape, and an external energy, representing the action of image data onto the model. Contour and surface models have been extensively studied for segmenting soft structures. Their extension to shape tracking through 2D or 3D image sequences has generally come to the use of the result at time point t as an initialization for the segmentation at time point $t + 1$ with some temporal smoothness constraints [14]. Image registration has been used as well to assist the initialization of the heart template, a crucial problem in such an approach. The extraction of both endocardial and epicardial cardiac surfaces is considered either as the coupled segmentation of two surfaces [14] or through the introduction of more complex volumetric models [21]. These latter models involve a volumetric representation of the heart associated to behavioral laws, such as elasticity. Level set methods, which can be closely linked with the previous deformable models, have also been investigated in this context [20, 6]. In this particular approach, however, the shape topology is allowed to change during the optimization process which is not always desirable. Another popular approach is based on prior learning or cardiac atlases. The prior model is a summary representation of the manual segmentation of a (great, as big as possible) number of patient data sets. One of the main difficulties is to be able to establish a unique correspondence between all the segmentations to build up the statical model [11, 16]. This statistical model then constrains the segmentation of the new data set through active shape (shape only)[13], active appearance models (taking into account image Grey levels) [18]. Filtering techniques are generally introduced to regularize the spatio-temporal segmentation [12, 15]. All these approaches present advantages and limitation. To our knowledge, no comparative studies have been conducted yet that could help selecting the optimal method for a specific context. We believe that prior models can greatly improve the segmentation. Here, a model is proposed that incorporates both physics and geometry. This model belongs to the volumetric deformable models. The initial model introduced in [21, 17] uses linear elasticity to deform the template. We

have developed a model which uses nonlinear elasticity. In this article, we demonstrate some important properties of the proposed volumetric model and associated numerical algorithms when displacements depend on the applied forces.

3. A nonlinear deformable elastic template

3.1. Description of the model

The approach adopted in this work for the segmentation of a smooth deformable object is based on prior assumptions about its shape. A geometric template represents the object interfaces as well as its interior and the elastic properties assigned to it. Within the image, the template is placed close to the structure one wants to extract (Figure 2). By applying a force field, the template is deformed and its edges are pulled to the borders of the targeted structure. The segmentation is achieved by the deformation of the template which is in turn achieved by the minimization of a global energy.

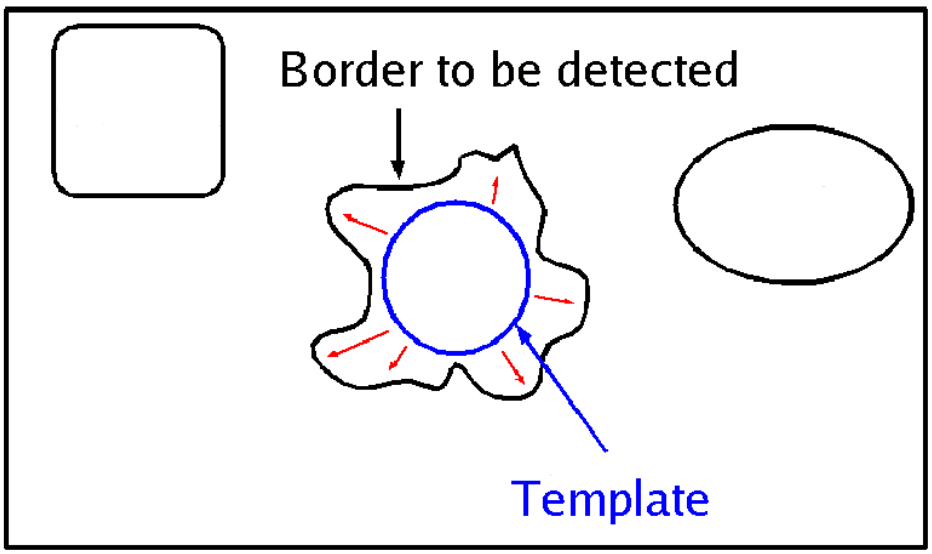

Figure 2. principle of the deformable models

The global energy to be minimized is composed of two terms. The first term is computed from the image data. Its role is to guide the deformation towards the border of the targeted object. The second term introduces a regularity constraint on the desired deformations. Its presence ensures also that the problem is settled in a suitable functional space.

In this article, the regularization term comes from the nonlinear elasticity, which allows large deformations. No part of the geometrical model is maintained fixed during the deformation process, which contributes to the automation of the segmentation.

The deformable model is generally formulated as a minimization of a functional. The equivalence between the minimization problem and local elasticity equations is

ensured when the material is hyper-elastic and the applied forces are conservative (i.e. derived from a potential energy, the exact definition is given in section 3.3).

For the considered applications the material of Saint Venat-Kirchhoff is considered which is hyper-elastic and the simplest model among all nonlinear models. It is also compatible with the physical hypotheses introduced in the next section. It is obtained by neglecting the higher-order terms in the expansion of the Piola-Kirchhoff stress tensor. The applied forces are assumed to be conservative. Let Ω be the domain to be deformed, $u : \overline{\Omega} \to \mathbb{R}^3$ and E be the following strain tensor

$$E(u) = \frac{1}{2}(\nabla u^t + \nabla u + \nabla u^t \nabla u), \tag{1}$$

A material of Saint Venat Kirchhoff is hyper-elastic and homogeneous, thus the strain energy is independent of a particular point $x \in \bar{\Omega}$ and defined by the relation

$$W(x, E) = W(E) = \frac{\lambda}{2} (\operatorname{Tr} E)^2 + \mu \operatorname{Tr} E^2 \tag{2}$$

Then the internal energy is defined for the reference state Ω by

$$E_{int}(u) = \int_\Omega W(\nabla(\mathbf{1} + u)(x))\, dx \tag{3}$$

While the external energy is expressed for the deformed state as:

$$E_{ext}(u) = -\int_{\partial\Omega} \hat{G}(\mathbf{1} + u)\, d\sigma \tag{4}$$

The function $\hat{G}$ is the potential of the applied surface forces. The methods used to compute the forces field are given in the application section 4. When the force field is conservative (see the definition in section 3.3), the minimization of the global energy

$$E_{total}(u) = E_{int}(u) + E_{ext}(u)$$

is "formally" equivalent to solving the Euler's equations (see section 3.3):

$$\begin{aligned} \operatorname{div}((\mathbf{1} + \nabla u)\Sigma(E(u))) &= 0 \quad \text{in } \Omega \\ -(\mathbf{1} + \nabla u)\Sigma(E(u)) \cdot \nu + g(u) &= 0 \quad \text{on } \partial\Omega \end{aligned} \tag{5}$$

where g is the applied surface forces, which is connected with a potential $\hat{G}$ by the relation (18), and Σ is a tensor defined by

$$\Sigma(E) = \lambda \operatorname{Tr}(E)\mathbf{1} + 2\mu E. \tag{6}$$

The Euler's equations (5) correspond to the pure traction elasticity problem of a Saint Venant Kirchhoff material with successive forces. In the following, equations (5) are studied in a general case when the material is not necessarily the Saint Venant Kirchhoff material. The nonlinear three-dimensional elasticity with boundary condition of pure traction is introduced and some preliminary results are given. Then an incremental algorithm is presented and its convergence is proved.

3.2. Notations and preliminary results related to the nonlinear elasticity problem with boundary condition of pure traction

The equilibrium equations are expressed in the reference configuration in terms of the first Piola-Kirchhoff stress tensor with the definition of an elastic material. More precisely, let Ω be a bounded open subset of $\mathbb{R}^3$, let ν be the unit outward normal to $\partial\Omega$ the boundary of Ω and let $a : \overline{\Omega} \times \mathbb{R}^{3\times 3} \to \mathbb{R}^{3\times 3}$, $h : \Omega \to \mathbb{R}^3$ and $g : \partial\Omega \to \mathbb{R}^3$ be a given functions with

$$a(x, \mathbf{1}) = 0, \quad \text{for all } x \in \overline{\Omega}. \tag{7}$$

Lanza de Cristophoris and Valent have established in [9] that there exists a value $r > 0$ such that, if $0 < \mu < r$ then there exists $u : \overline{\Omega} \to \mathbb{R}^3$ solution of

$$\begin{aligned} &\mathrm{div} A(u) + \mu h = 0 \quad \text{in } \Omega \\ &-A(u)\nu + \mu g = 0 \quad \text{on } \partial\Omega \end{aligned} \tag{8}$$

where $A(u)(x) = a(x, \mathbf{1} + \nabla u(x))$ with $\nabla u(x) = (\partial_j u_i(x))_{i,j=1,2,3}$ is the gradient of u and $A(u)\nu$ is the function from $\partial\Omega$ with values in $\mathbb{R}^3$ defined by

$$(A(u)\nu)_i(x) = \sum_{j=1}^{3} a_{ij}(x, \mathbf{1} + \nabla u(x))\nu_j(x) \quad i = 1, 2, 3.$$

The equations (8) correspond to the pure traction problem of nonlinear elasticity. In the physical context, Ω represents the reference configuration of an elastic body, u is the displacement, $\mathbf{1} + u$ the deformation corresponding to u. The function a defines the response of the material, and $a(x, \mathbf{1} + \nabla u(x))$ is the first Piola-Kirchhoff stress tensor at the point $x \in \Omega$. The function g is the surface traction per unit surface area in the reference configuration Ω. Throughout this work n, m denotes non negative integers and p denotes a real number greater than one. $L^p(\Omega)$ is the space of (classes of) measurable functions $v : \Omega \to \mathbb{R}$ such that $|v|^p$ is Lebesgue-integrable, while $W^{m,p}(\Omega)$ is the (Banach) space of elements v of $L^p(\Omega)$ equipped with the norm

$$\|v\|_{m,p} = \sum_{|\alpha|\leq m} \|D^\alpha v\|_{0,p},$$

where $\|\cdot\|_{0,p}$ is the usual $L^p(\Omega)$ norm. If Ω has the cone property, and if $mp > 3$, then $W^{m,p}(\Omega)$ is a Banach algebra (see [1]), i.e.,

$$u, v \in W^{m,p}(\Omega) \Rightarrow uv \in W^{m,p}(\Omega), \|uv\|_{m,p} \leq c_{m,p}\|u\|_{m,p}\|v\|_{m,p},$$

where $c_{m,p}$ is a positive number independent of u and v (see [1], Th. 5.23). If $v = (v_i)_{i=1,2,3}$ belongs to $(W^{m,p}(\Omega))^3$ we take :

$$\|v\|_{m,p} = \sum_{i=1}^{3} \|v_i\|_{m,p}$$

We set $V = (W^{m+2,p}(\Omega))^3$, $X = (W^{m,p}(\Omega))^3 \times (W^{m+1-1/p,p}(\partial\Omega))^3$. Let the operator $L : V \longrightarrow X$, be defined by

$$u \longmapsto L(u) = (\mathrm{div}(A(u)), A(u)\nu)$$

Then the problem of pure traction (8) can be written as

$$L(u) = \mu f, \tag{9}$$

where

$$f = \begin{pmatrix} -h \\ g \end{pmatrix} \in X.$$

The following spaces

$$\begin{aligned} V_{m,p} &= \left\{ v \in (W^{m+2,p}(\Omega))^3 \ : \ \int_\Omega v \mathrm{d}x = 0, \ \int_\Omega (\partial_j v_i - \partial_i v_j)\mathrm{d}x = 0, \ {}_{i,j=1,2,3.} \right\} \\ F_{m,p} &= \left\{ (h,g) \in (W^{m,p}(\Omega))^3 \times (W^{m+1-1/p,p}(\partial\Omega))^3 \ : \ (h,g) \text{ is equilibrated} \right\} \end{aligned} \tag{10}$$

are used in [9] to prove the existence and uniqueness results. For the convenience of the reader, a precise statement of those results is given in the Appendix.

In the next section, an incremental algorithm is given to compute an approximation of the solution of the pure traction problem with successive forces (the functions h and g depend on the displacements u). The convergence of the algorithm is proved.The incremental method permitted also to extend the existence and uniqueness results of Lanza De Cristoforis and Valent [9] to the problem of successive forces, and to give another proof of their results.

3.3. Incremental method for nonlinear elasticity in pure traction with successive forces

Let h be a vector field defined in Ω. To segment the images, we need a vector field g defined in the domain $\mathcal{O}$ containing $\bar{\Omega}$. The equilibrium equations in pure traction with successive forces written in the reference configuration read:

$$\begin{aligned} &\mathrm{div}A(u) + h(u) = 0 \quad \text{in } \Omega \\ &-A(u)\nu + g(u) = 0 \quad \text{on } \partial\Omega \end{aligned} \tag{11}$$

or

$$L(u) = f(u) \quad \text{in } \Omega \times \partial\Omega, \tag{12}$$

with $L(u) = (\mathrm{div}A(u), A(u)\nu)$. In the sequel, it is assumed that f is a $\mathcal{C}^2(V_{m,p}; F_{m,p})$ function. The notations are those given in section 3.2.

Let us introduce the incremental method originally proposed by Ciarlet [7] for the case of pure displacement with forces independent of the displacement. The incremental method is based on the introduction of a sequence of parameterized problems. Hereafter,

some technical results are given which prove the convergence of the incremental method. For $\lambda \in [0,\, 1]$, define $u(\lambda)$ as the solution to

$$L(u(\lambda)) = \lambda f(u(\lambda)) \quad \text{in } \Omega \times \partial\Omega \tag{13}$$

After differentiating this relation with respect to λ and adding an initial condition, we obtain

$$\begin{aligned} &u'(\lambda) = (L'(u(\lambda)) - \lambda f'(u(\lambda)))^{-1} f(u(\lambda)),\ 0 \le \lambda \le 1, \\ &u(0) = 0. \end{aligned} \tag{14}$$

We have

Lemma 3.1 *Assume that Ω is a $\mathcal{C}^{m+2}$ bounded domain, $pm > 3$, that $a \in (\mathcal{C}^{m+3}(\bar{\Omega} \times \mathbb{R}^{3\times 3}))^{3\times 3}$, and that hypotheses (A.1) apply. If there exists $\rho > 0$ and a constant K such that $|f'(v)|_{\mathcal{L}(V;X)} \le K\|v\|_{m+2,p}$ for all v belonging to the ball $\mathcal{B}(0,\rho_1)$ with the radius ρ_1, then there exists ρ_2 such that the operator $(L'(u) - \lambda f'(u))$ is invertible for all u in the ball $\mathcal{B}(0,\rho_1)$ in $V_{m,p}$.*

Proof. Although one is in infinite dimension, there exists $\rho > 0$ such that for all $\|v\|_{m+2,p} \le \rho$, $L'(v)$ is an isomorphism. In fact, from the lemma Appendix A.2 $L'(0)$ is an isomorphism from $V_{m,p}$ onto $F_{m,p}$. The spaces $V_{m,p}$ and $F_{m,p}$ being defined with the relation (10), we can write

$$L'(v) = L'(0)(\mathbf{1} - (L'(0))^{-1}(L'(0) - L'(v))),$$

The operator defined by $T_v = (L'(0))^{-1}(L'(0) - L'(v))$ is linear and continuous from $V_{m,p}$ in $V_{m,p}$ for all $v \in V_{m,p}$. With application of the mean value theorem and Lemma Appendix A.1, we get

$$\begin{aligned} |T_v|_{\mathcal{L}(V)} &\le |L'(0)^{-1}|_{\mathcal{L}(X;V)} |L'(0) - L'(v)|_{\mathcal{L}(V;X)} \\ &\le |L'(0)^{-1}|_{\mathcal{L}(V,X)} \sup_{\|v\|_V \le \rho} |L''(v)|_{\mathcal{L}(V;\mathcal{L}(V;X))} \|v\|_V \\ &\le M_1 M_2^{\rho} \|v\|_V \end{aligned}$$

M_1 stands for the norm of $L'(0)^{-1}$ and M_2^{ρ} is a constant resulting from the Lemma Appendix A.1. Let ρ be a strictly positive number such that

$$\rho_2 < \min(\frac{1}{M_1 M_2}, \rho). \tag{15}$$

Then $|T_v|_{\mathcal{L}(V)} < 1$ for all v in the ball $\mathcal{B}(0,\rho_2)$, it follows that the operator $L'(v) = L'(0)(\mathbf{1} - T_v)$ is an isomorphism of $V_{m,p}$ onto $F_{m,p}$. Let us prove that there exists ρ_2 such that $L'(u) - \lambda f'(u)$ is invertible for $\|v\|_{m+2,p} \le \rho_2$. For $\|v\|_{m+2,p} \le \rho$ we have the relation

$$L'(u) - \lambda f'(u) = L'(u)(\mathbf{1} - \lambda L'(u(\lambda))^{-1} f'(u(\lambda)))$$

Set $T_u = \lambda L'(u)^{-1} f'(u)$. Since there exists a $\rho_1 > 0$ and a constant K such that for $\|u\|_{m+2} < \rho_1$

$$|f'(u)|_{\mathcal{L}(V;X)} \leq K\|u\|_{m+2,p},$$

it follows that

$$|T_u|_{\mathcal{L}(V)} \leq KM\|u\|_{m+2,p}$$

M stands for the norm of $L'(u)^{-1}$. Then $L'(u) - \lambda f'(u)$ is an isomorphism from $V_{m,p}$ into $F_{m,p}$ for all $\|u\|_V \leq \rho_1$ such that $\rho_1 < \min\,(\frac{1}{KM};\, \rho;\, \rho_2)$.

■

Let $B(u) = L'(u) - \lambda f'(u)$

Lemma 3.2 *Assume that Ω is $\mathcal{C}^{m+2}$, $pm > 3$, $a \in (\mathcal{C}^{m+3}(\bar{\Omega} \times \mathbb{R}^{3\times 3}))^{3\times 3}$ and that the hypotheses (A.1) apply. If there exists a $\rho_1 > 0$ and a constant K such that $|f'(v)|_{\mathcal{L}(V;X)} \leq K\|v\|_{m+2,p}$ for all v in the ball $\mathcal{B}(0,\rho_1)$, then there exists a $\rho > 0$ such that $B(u)^{-1}f(u)$ is Lipschitzian in the ball $\mathcal{B}(0,\rho)$; more precisely, there exists a constant C such that : $\forall u_1, u_2$ satisfying $\|u_1\|_V < \rho,\ \|u_2\|_V < \rho$:*

$$|B(u_1)^{-1}f(u_1) - B(u_2)^{-1}f(u_2)|_{\mathcal{L}(X;V)} \leq C\|u_1 - u_2\|_V. \tag{16}$$

Proof. Given the two elements $\|u_1\|_V \leq \rho_2$, $\|u_2\|_V \leq \rho_2$, we have the factorizations

$$\begin{aligned}
&B(u_1)^{-1} - B(u_2)^{-1} = B(u_1)^{-1}(B(u_2) - B(u_1))B(u_2)^{-1}\\
&B(u_1)^{-1}f(u_1) - B(u_2)^{-1}f(u_2) = (B(u_1)^{-1} - B(u_2)^{-1})f(u_1) +\\
&\qquad B(u_2)^{-1}(f(u_1) - f(u_2));
\end{aligned}$$

the previous relations combined with the mean value theorem lead to

$$\begin{aligned}
\|B(u_1)^{-1}f(u_1) - B(u_2)^{-1}f(u_2)\| &\leq \|B(u_1)^{-1} - B(u_2)^{-1}\|\|f(u_1)\| +\\
&\quad \|B(u_2)^{-1}\|\|f(u_1) - f(u_2)\|\\
&\leq k_1\|B(u_1)^{-1}(B(u_2) - B(u_1))B(u_2)^{-1}\| +\\
&\quad M_1K\rho_1\|u_1 - u_2\|\\
&\leq k_1M_1^2\|B(u_2) - B(u_1)\| + M_1K\rho_1\|u_1 - u_2\|\\
&\leq (k_1k_2M_1^2 + M_1K\rho_1)\|u_1 - u_2\|
\end{aligned}$$

■

Corollary 3.3.1 *Assume that Ω is $\mathcal{C}^{m+2}$, $pm > 3$, $a \in (\mathcal{C}^{m+3}(\bar{\Omega} \times \mathbb{R}^{3\times 3}))^{3\times 3}$ and that hypothesis (A.1) applies. If there exists $\rho_1 > 0$ and a constant K such that $|f'(v)|_{\mathcal{L}(V;X)} \leq K\|v\|_{m+2,p}$ for all v in the ball $\mathcal{B}(0,\rho_1)$, then the differential equation (14) has one and only one solution. This solution is also a solution of $L(u(\lambda)) = \lambda f(u(\lambda))$ up to $\lambda = 1$.*

Proof. Using the lemma 3.1 and 3.2, we verify that the mapping

$$\Phi\ :\ u \in \mathcal{C}^0([0,\,1];\mathcal{B}(0,\rho)) \to \Phi(u) \in \mathcal{C}^0([0,\,1];V_{m,p})$$

with

$$\Phi(u)(\lambda) = \int_0^\lambda \Big(L'(u(\mu)) - \mu f'(u(\mu))\Big)^{-1} f(u(\mu))\,\mathrm{d}\mu$$

is well defined and : $\lambda \in [0,\ 1] \to \Big(L'(u(\lambda)) - \lambda f'(u(\lambda))\Big)^{-1} \in V_{m,p}$ is continuous, since it is composed of several continuous mappings. Then for $u \in \mathcal{C}^0([0,\ 1]; \mathcal{B}(0,\rho))$ we have $\Phi(u) \in \mathcal{C}^0([0,\ 1]; V_{m,p})$. In addition, if the vector space $\mathcal{C}^0([0,\ 1]; V_{m,p})$ is equipped with the norm

$$|||\Psi||| := \sup_{0\le\lambda\le 1} \|\Psi(\lambda)\|_{2+m}$$

it becomes a Banach space, so that a subset of $\mathcal{C}^0([0,\ 1]; \mathcal{B}(0,\rho))$ is a complete metric space.
Using the lemma 3.1 and 3.2, the mapping Φ or an iterate thereof: $\Phi^k = \Phi(\Phi(\ldots))$ is a contraction of the space $\mathcal{C}^0([0,\ 1]; \mathcal{B}(0,\rho))$. According to the contraction mapping theorem, there exists a unique fixed point of the contraction Φ^k and consequently this point is the unique solution of (14).

In addition, for a u solution of the differential equation (14) we have

$$0 = L'(u(\lambda))u'(\lambda) - f(u(\lambda)) - \lambda f'(u(\lambda))u'(\lambda) = \frac{d}{d\lambda}(L(u(\lambda)) - \lambda f(u(\lambda)))$$

from which we deduce that

$$\lambda \in [0,\ 1] \to (L(u(\lambda)) - \lambda f(u(\lambda)))$$

is a constant mapping, which vanishes since $u(0) = 0$, i.e. u is a solution of the equation

$$L(u(\lambda)) = \lambda f(u(\lambda)) \text{ with } 0 \le \lambda \le 1.$$

■

Theorem 3.1 *Assume that the hypotheses of the corollary 3.3.1 apply, and let* $(\lambda_n)_{n\in\mathbb{N}}$ *be a sequence in* $[0,1]$. *Then there exists a sequence* $(u_n)_{n=1}^{n=N}$ *satisfying*

$$\begin{aligned} &u_0 = 0,\ 0 \le n \le N, \\ &(L_1'(u_n) - \lambda_n h'(u_n))(u_{n+1} - u_n) = (\lambda_{n+1} - \lambda_n)\, h(u_n) \ \textit{in} \quad \Omega \\ &(L_2'(u_n) - \lambda_n g'(u_n))(u_{n+1} - u_n) = (\lambda_{n+1} - \lambda_n)\, g(u_n) \ \textit{on} \quad \partial\Omega. \end{aligned} \tag{17}$$

Moreover, there exists a constant c *such that*

$$\|u_n - u(\lambda_n f)\| \le c\,(\lambda_{n+1} - \lambda_n),$$

where $u(\lambda_n f)$ *denotes the unique solution in the ball* $\mathcal{B}(0,\rho)$ *of the equation* $L(u) = \lambda_n f(u)$.

Proof. This algorithm corresponds to an Euler's method to approximate the solution of the equations (14). Due to lemma 3.2, this problem satisfies the hypotheses of the convergence of Euler's method :

- $u \to \Big(L'(u) - \lambda f'(u)\Big)^{-1} f(u)$ is Lipschitzian in the ball $\mathcal{B}(0,\rho)$;
- $\lambda \in [0,1] \to \Big(L'(u(\lambda)) - \lambda f'(u(\lambda))\Big)^{-1} f(u(\lambda)) \in V_{m,p}$ is continuous, since it is composed of several continuous mappings.

Since the longest step $(\lambda_{j+1} - \lambda_j)$ of the sequence $(\lambda_j)_j$ tends towards 0, the algorithm (17) converges (see [8]). ■

Now let us specify in which circumstance the apply forces are conservative. The applied force fields h and g are conservative if there exists two potential forces $\hat{F} : \Omega \times \mathbb{R}^3 \to \mathbb{R}$ and $\hat{G} : \partial\Omega \times \mathbb{R}^3 \times \mathbb{R}_+^{3\times 3} \to \mathbb{R}$ such that the functionals defined by

$$F(\psi) = \int_\Omega \hat{F}(x, \psi(x))\, dx \;\text{ and }\; G(\psi) = \int_{\partial\Omega} \hat{G}(x, \psi(x), \nabla\psi(x))\, d\sigma(x)$$

have the following Gâteaux derivatives

$$F'(\phi)\theta = \int_\Omega h(\phi(x)) \cdot \theta(x)\, dx \;\text{ and }\; G'(\phi)v = \int_{\partial\Omega} g(\phi(x)) \cdot v(x)\, d\sigma(x) \quad (18)$$

An elastic material with the response function a $\bar{\Omega} \times \mathbb{R}_+^{3\times 3} \to \mathbb{R}^{3\times 3}$ is hyper-elastic if there exists a function $W : \bar{\Omega} \times \mathbb{R}_+^{3\times 3} \to \mathbb{R}$, differentiable with respect to the variable $F \in \mathbb{R}_+^{3\times 3}$ for each $x \in \bar{\Omega}$, such that

$$a_{ij}(x, F) = \frac{\partial W}{\partial F_{ij}}(x, F),\ 0 \le i, j \le 3$$

The function W is called the stored energy function.
Finally we end this section with a result proved in [7].

Theorem 3.2 *We consider an hyper-elastic material and assume that the applied forces are conservative. Let*

$$\mathcal{U} = \{\psi : \bar{\Omega} \to \mathbb{R}^3, det\nabla\psi > 0, \int_\Omega \psi dx = e\}$$

The boundary value problem is "formally" equivalent to the minimization problem:

$$\phi \in \mathcal{U} \text{ and } I(\phi) = \inf_{\psi\in\mathcal{U}} I(\psi),$$

where

$$I(\psi) = \int_\Omega W(x, \nabla\psi(x))\, dx - (F(\psi) + G(\psi)),$$

and W is a strain energy for a hyper-elastic problem.

This theorem allows us to formulate the pratical algorithm for DET based segmentation. In the next section, the incremental method is applied to image segmentation.

4. Application of the incremental method to image segmentation

To apply the incremental method to image segmentation, the St Venant-Kirchhoff material is used. Note that this is the simplest model among all nonlinear models and that it is compatible with the hypotheses introduced previously. The notations introduced at the beginning of the previous section are used. The strain energy is independent of a particular point $x \in \bar{\Omega}$ and defined by the relation

$$W(E) = \frac{\lambda}{2} (\mathrm{Tr}\, E)^2 + \mu\, \mathrm{Tr}\, E^2. \tag{19}$$

Then the internal energy is defined for the reference state Ω by

$$E_{int}(u) = \int_{\Omega} W(\nabla(\mathbf{1} + u)(x))\, \mathrm{d}x. \tag{20}$$

While the external energy is expressed for the deformed state as:

$$E_{ext}(u) = -\int_{\partial\Omega} \hat{G}(\mathbf{1} + u)\, \mathrm{d}\sigma. \tag{21}$$

The function $\hat{G}$ is the potential of the applied surface forces.

When the force field is conservative, the minimization of the total energy

$$E_{total}(u) = E_{int}(u) + E_{ext}(u)$$

is "formally" equivalent to solving the Euler's equations (see previous section). These equations are the equilibrium equations of a St Venant-Kirchhoff material:

$$\begin{aligned} \mathrm{div}((\mathbf{1} + \nabla u)\Sigma(E(u))) &= 0 \quad \text{in } \Omega \\ -(\mathbf{1} + \nabla u)\Sigma(E(u)) \cdot \nu + g(u) &= 0 \quad \text{on } \partial\Omega \end{aligned}$$

The force field g and the potential $\hat{G}$ are connected by relation (18).

For instance, it can be computed from the norm of the image gradient, an edge map obtained using a Canny operator [5] smoothed with a Gaussian filter, or a distance map [3], [24]. The Gradient Vector Flow algorithm (GVF) introduced in [26] generates a force field by an iterative diffusion process, which is not derived from a potential. The force field obtained by the GVF method is not conservative, but if used it in the equations (5) below, the numerical results are equivalent as the results obtained with the Canny technique. For the convenience of the reader, let us briefly recall the main features of the Gradient Vector Flow method. One of the aims of the GVF is to extend the force field extracted from the gray level function with a diffusion process. If I denotes the gray level function of the image defined everywhere, the GVF method can be summarized in three steps.

1- Regularize with a smooth convolution kernel the function I, which is still denoted by I.

2- Compute the edge map $p(x) = \|\nabla I(x)\|^2$ and set to zero the values of ∇p greater than a fixed large parameter.
3- Extend ∇p in a bounded domain $\mathcal{O}$ containing the image of interest with a diffusion process. For a fixed inverse-diffusion parameter μ_{GVF}, compute solution $\mathbf{f}$ of

$$\begin{array}{cc} \Delta \mathbf{f} - \mu_{GVF}(\mathbf{f} - \nabla p)\|\nabla p\|^2 = 0 & \text{in } \mathcal{O}; \\ \mathbf{f} = 0 & \text{on } \partial\mathcal{O}. \end{array} \tag{22}$$

Roughly speaking, when $\|\nabla p\|^2$ is large, $\mathbf{f} = \nabla p$, and outside of these regions, $\mathbf{f}$ is extended in a smooth way.

The MR images of the mice used for the application in section 5 contained many small features (papillary muscles, coronaries, ect.). Therefore, mophological filtering ang GVF were used to pre-process the images and compute the force field acting onto the model, see [25].

To segment a simple structure, an explicit force field can be computed. For example to segment a sphere with the radius 1 from one image, the following force field can be used

$$g(x) = -\alpha(\|x\| - 1)\frac{x}{\|x\|}$$

with $0 < \alpha < 1$.

4.1. Finite Element Discretization

In this section, an algorithm to compute the solution of the problem (5) is given. Using the notation introduced previously, the parameterized problem associated to (5) can be written as $L(u(\lambda)) = \lambda\, f(u(\lambda))$, where

$$f(u) = \begin{pmatrix} 0 \\ g(u) \end{pmatrix}.$$

For the numerical implementation of this algorithm, the finite element method is used. Let M be a positive number, $\{\psi_1, \cdots, \psi_M\}$ the basis for an approximation of the displacement in $V_{m,p}$ and $V_h = Vect\{\psi_1, \cdots, \psi_M\}$.
The variational problem associated to the incremental method is the following: Given u_n, find a $u_{n+1} \in V_h$ which is a solution of

$$\begin{aligned} \int_\Omega k(u_n, u_{n+1}) : \nabla v \,\mathrm{d}x - \lambda_n \langle g'(u_n) \cdot u_{n+1}, v\rangle = \int_\Omega k(u_n, u_n) : \nabla v \,\mathrm{d}x \\ -\lambda_n \langle g'(u_n) \cdot u_n, v\rangle + (\lambda_{n+1} - \lambda_n) \int_{\partial\Omega} g(u) v \,\mathrm{d}\sigma \quad \forall v_h \in V_h. \end{aligned} \tag{23}$$

where

$$k(u, w) = (\mathbf{1} + \nabla u)\Sigma(\epsilon(w) + \frac{1}{2}(\nabla u^t \nabla w + \nabla w^t \nabla u)) + \nabla w \Sigma(\mathbf{E}(u)),$$

which is a linearization of the tensor

$$K(u) = (\mathbf{1} + \nabla u)\Sigma(E(u)).$$

at w (i. e. k(u,w)= K'(u)w). The scalar product $< \cdot, \cdot >$ is defined on $\partial\Omega$ for the two functions α and β by :

$$< \alpha, \beta >= \int_{\partial\Omega} \alpha(x)\beta(x)\mathrm{d}\sigma.$$

Resolution algorithm

Let U_O a vector containing displacement components.

- Initialization step
$$U_O = 0 \quad \text{and} \quad u_0 = 0;$$
- Iterations
  (i) Assemble the rigidity matrix at iteration n
$$\mathcal{K}^n_{ij} = \int_{\Omega_h} k(u_n, \psi_i, \lambda_n) : \nabla\phi_j \,\mathrm{d}x - \langle g'(u_n) \cdot \psi_i, \psi_j \rangle, \quad 1 \leq i, j \leq M;$$
  (ii) Solve the linear system derived from (23), with U_{n+1} as an unknown
$$\mathcal{K}^n U_{n+1} = \mathcal{K}^n U_n + (\lambda_{n+1} - \lambda_n)\mathcal{F}(U_n);$$
  (iii) Compute the approximate displacement at iteration $n + 1$
$$u_{n+1} = \sum_{i=1}^{i=M} U_{n+1,i}\,\psi_i;$$
  (iv) If $\|u_{n+1} - u_n\| < \epsilon$ stop, otherwise go to (i).

In this algorithm, the matrix $\mathcal{K}^n$ is updated at each iteration, the iterations require therefore much computing time. The convergence of the algorithm can be accelerated by updating the rigidity matrix $\mathcal{K}^n$ only after several iterations instead of updating it at each iteration. So, a step time sequence $(\tau_1, \tau_2, \ldots, \tau_n)$ is introduced, called super-step in reference to the super-step method described in [10]. Now, let $U^0 = 0$ and compute $U^{n(N+1)+1} \in \mathbb{R}^M$ such that :

- for $k = 0, 1, \cdots, N$
  - for $i = 0, 1, \cdots, n$
$$\mathcal{K}^k U^{i+nk+1} = \mathcal{K}^k U^{i+nk} - \tau_{i+1}\mathcal{F}(U^{i+nk});$$
  - end i
- end k

Two types of iterations are used : internal and external iterations. With the external iterations, the rigidity matrix is updated, which permits one to carry out large displacements. Internal iterations do not require the computation of the matrix. Hence, less computing time is needed for internal iterations than for external iteration. The number of external iterations should be therefore reduced as much as possible. This can be achieved by compensating with internal iterations. However, several external iterations are needed for large displacements. The number of required external iterations depends on the problem. If only small displacements are required it is unnecessary to update the rigidity matrix. In that case, internal iterations are sufficient.

4.2. Tests

To evaluate the method, an example with a known target object is considered. A sphere (see Fig 3-(b)) is transformed into an ellipsoid, i. e. the template is a sphere and the target border is an ellipsoid. The axis of the ellipsoid are chosen in such way that the transformation demands large displacements. A force field is computed from the image (see Fig 3-(a)). The mesh representing the template has 15 019 tetrahedrons and 3 003 nodes and satisfies the quality conditions introduced in [4].
The segmentation result obtained with the proposed method is shown in Fig 3-(c). The nonlinear elasticity was replaced by linear elasticity. Note that the linear model is unable to correctly detected the ellipsoid (see Fig 3-(d)).

5. Simultaneous Segmentation of the left and right Heart Ventricles in 3D Cine MR Images

5.1. Experimental data

Mouse cine MR images were acquired with a 7 T magnetic resonance scanner with a whole body coil for RF excitation and a 15 mm surface coil for MR signal reception. An ECG-gated FLASH sequence was used to acquire short-axis cine images with 25 mm^2 FOV, 256×256 pixels, 1 mm slice thickness, 7/3.5 ms TR/TE, 64 KHz bandwidth and 20 degrees flip-angles. Cine images (16 frames over the cardiac cycle) were acquired for 7 slice levels, covering the entire LV (left ventricle). With a cardiac frequency of 450 b.p.m, the total acquisition time was 20 minutes.

5.2. Image data preprocessing

High resolution MR images have a relatively low SNR. Furthermore, the abundance of small features in the images (papillary muscles, coronaries, etc.) can lead to local minima of the model energy, leading to inaccurate segmentation. Both problems need to be addressed before the image edges can be extracted. We applied morphological opening to remove small features and noise while preserving strong edges (see [25]).

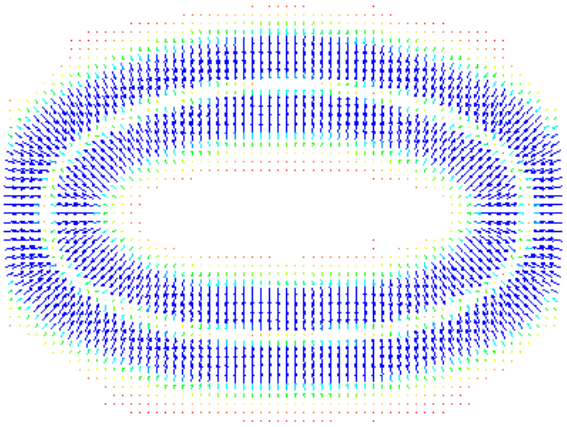

(a)

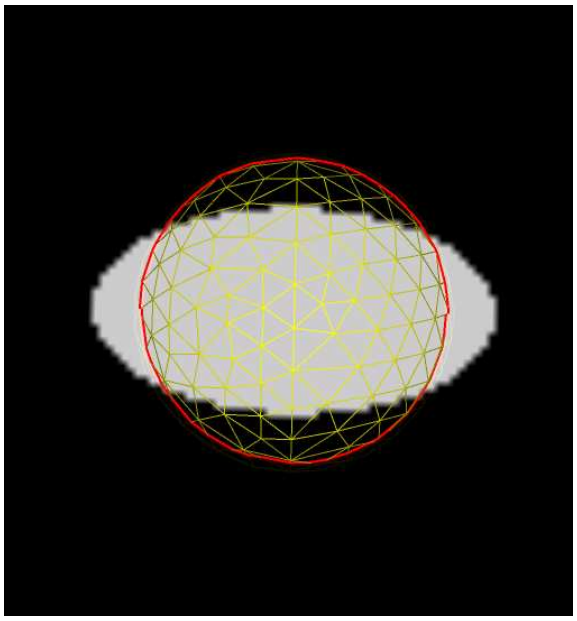

(b)

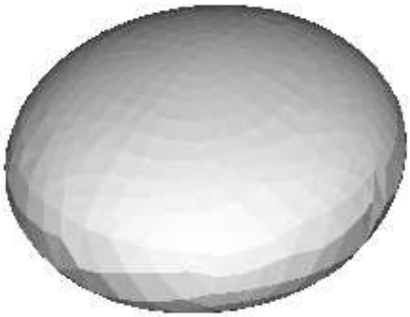

(c)

(d)

Figure 3. (a): 2D plane section of the 3D force field, (b): initial templat and targret ellipsoid, (c): result obtained with nonlinear DET, (d): result obtained with linear DET.

5.3. Results

Four 4D MRI sequences corresponding to 4 different mice were processed using our method. The parameters of the model were a Young modulus of 10 Pa for the LV (left ventricle) and 40 Pa for the RV (right ventricle), and a Poisson coefficient of 0.485 for the whole model. Results show that although we are still experiencing a few specific problems, our method is able to correctly locate the heart in the images and retrieve its contours. Figure 4 illustrates the 3D segmentation process. Figure 5-(a)-(b) shows the results of the deformation of the 3D mesh of the same 3D image.

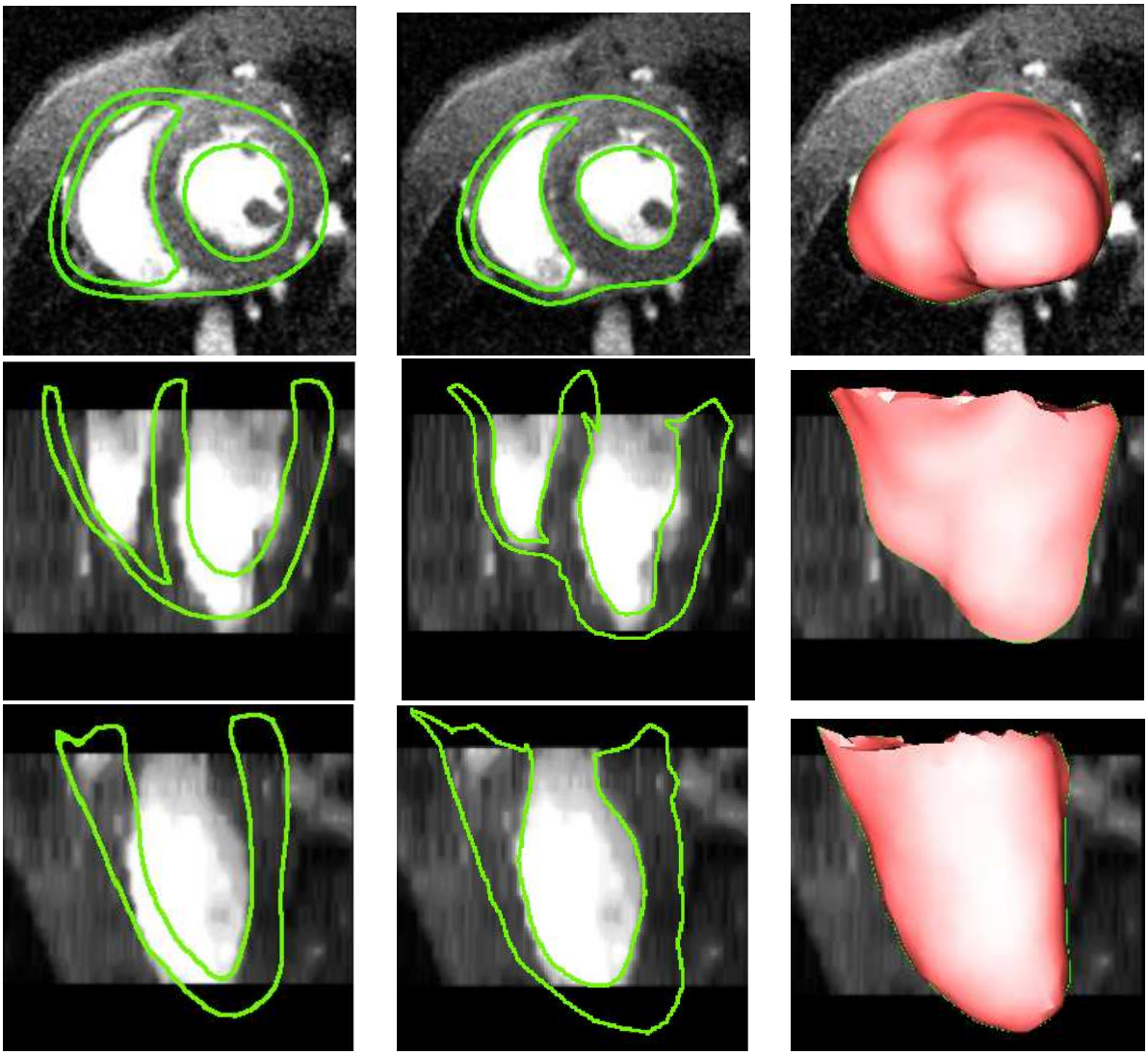

(a) (b) (c)

Figure 4. Segmentation of the heart ventricles in MR images of the mouse. Column (a): trace of initial model, orthogonal slices with Z, X and Y after affine registration of the model, column (b): trace of the deformed model after segmentation using DET model, column (c): 3D deformed model according to the three directions.

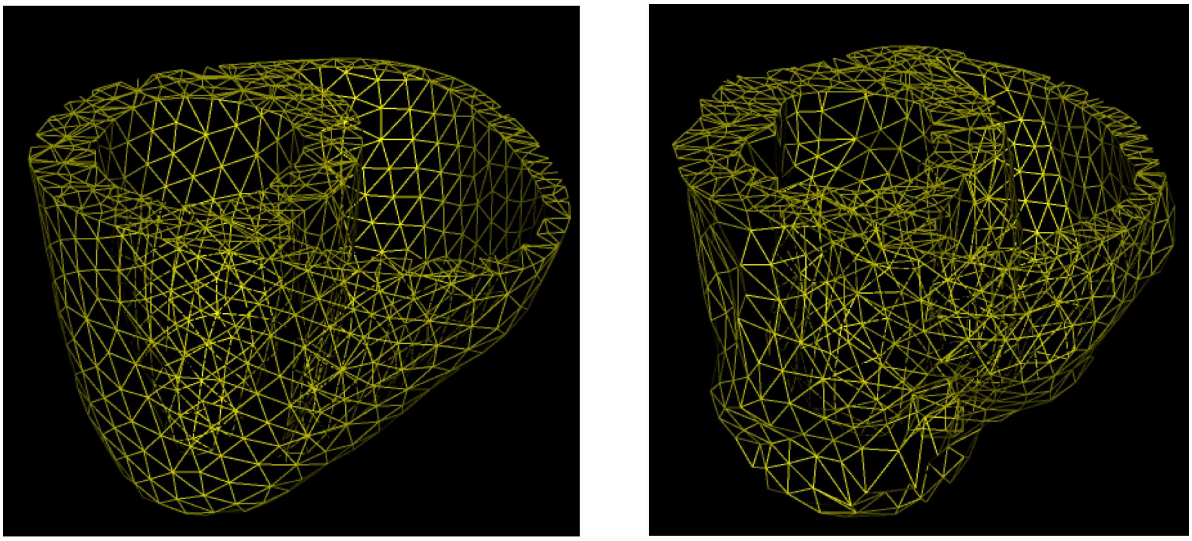

(a) (b)

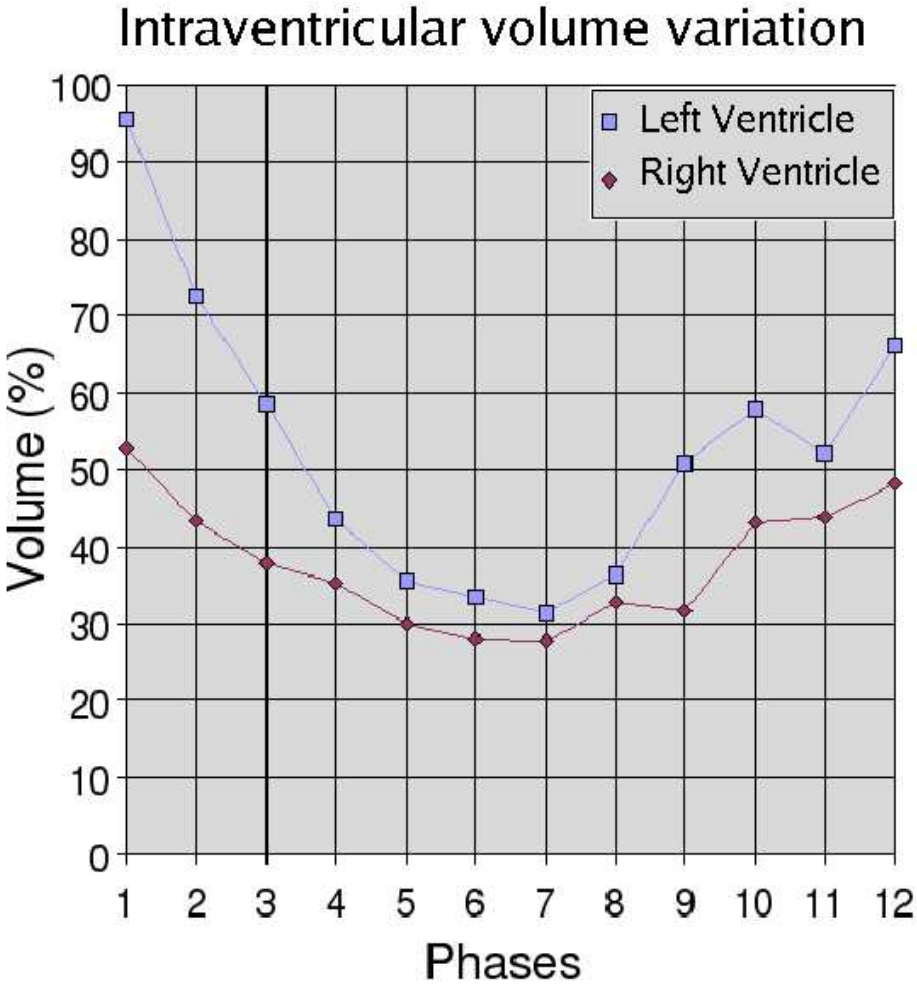

Figure 5. (a) Original model and (b)deformed model; Diagram on the bottom: Estimated volume variation of the ventricles over the cardiac cycle.

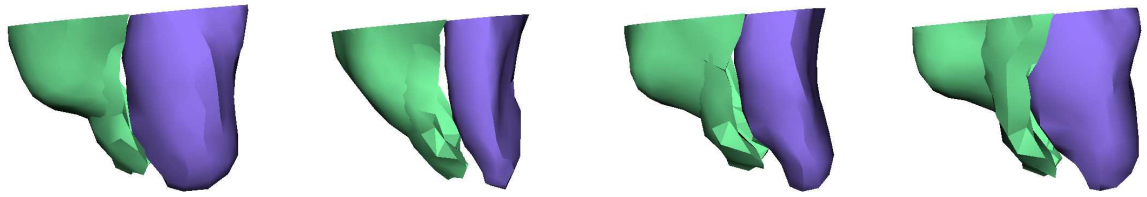

Figure 6. Tracking of the ventricular cavities of a mouse during a cardiac cycle (4 phases separated by 64 ms intervals).

One direct application of segmentation is the automatic extraction of the ventricle cavity volumes over the cardiac cycle. Segmentation tracking of the heart is achieved by taking the segmentation result at the present time frame at the initial solution at the next time frame, and repeating the process for all the times frames of the MRI sequence. Once the 3D contours have been extracted, it is easy to compute the enclosed volumes. Figure 5 shows on the right hand an example of volume variation curves obtained by automatic segmentation tracking. Figure 6 shows the obtained model at frame time points. The overall variation pattern is coherent. However, localized problems persist during early diastole. These problems may be solved using temporal constraints for the segmentation tracking.

6. Discussion and conclusions

The main contribution of this article is the derivation of convergence results for the incremental method, which is used to approximate a solution for a 3D nonlinear elastic template under successive forces. This sets a convenient framework for the segmentation of soft structures in 3D and 3D+time images. Experiments were conducted with both synthetic and medical images showing the practical behavior of the proposed model.

The proposed method was able to retrieve the heart contours in most cases, allowing the computation of volume variation curves. However, manual interaction and correction of the results would still be needed to use the method routinely experiments. Remaining problems include inaccuracies in the segmentation of the pericardium due to the presence of numerous anatomical structures close to the heart, and localized errors during the early diastolic phase due to motion artifacts. Another aspect concerns the papillary muscle which might be included into the myocardium segmentation as shown in Figure 7.

Note that for the segmentation of a cardiac cycle progressive segmentation (see section 5.4) was used. It will be interesting to include a temporal constraint in the model by introducing non stationary equations for the segmentation over the cardiac cycle. Larger scale experiments, including quantitative evaluation of the segmentation accuracy will also be needed to fully validate the method.

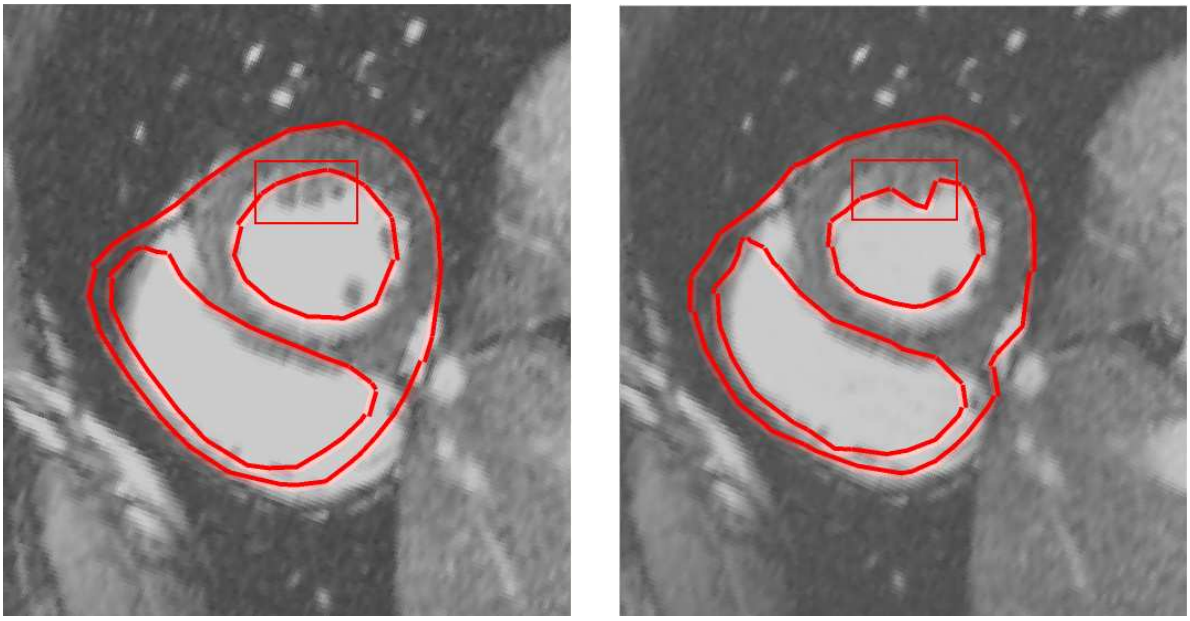

Figure 7. On the left hand: trace of the initial model; On the right hand: trace of the deformed model

Appendix A. Proprieties of elasticity pure traction problem

Table A1. Notations.

Ω	bounded open subset of $\mathbb{R}^3$
$\partial\Omega$	boundary of Ω
m, p, n	integer numbers
$\|\cdot\|_{m,p}$	norm of $Wm,p(\Omega)$
ν	the unit outward normal to Ω
g	applied surface forces
h	applied volume forces
a	$\overline{\Omega}\times\mathbb{R}^{3\times3}\to\mathbb{R}^{3\times3}$: response of material expressed in terms of the first Piola-Kirchhoff stress tensor
$E(u)$	$E(u)=\frac{1}{2}\big(\nabla u^t+\nabla u+\nabla u^t\nabla u\big)$: Strain tensor
$W(E)$	$W(E)=\frac{\lambda}{2}\big(\operatorname{Tr}(E)\big)^2+\mu\operatorname{Tr}(E^2)$: strain energy of St-Venant Kirchhoff
Q	set of orthogonal matrices of $\mathbb{R}^{3\times3}$
M^t	transpose of the M matrix.

Appendix A.1. hypotheses and results

Let $\sigma=(\sigma_{ij})_{i,j=1,2,3}\in\mathbb{R}^{3\times3}\setminus\{0\}$ be a tensor with $\sigma_{ij}=\sigma_{ji}$. According to the physical context, it is assumed that a satisfies the following hypotheses

$$a(x,qy)=qa(x,y)q^t \quad \text{for all} \quad (x,y)\in\overline{\Omega}\times\mathbb{R}^{3\times3} \text{ and } q\in \mathrm{Q},$$

derived from the principle of material frame-indifference, and

$$a(x,y)y^t=ya^t(x,y) \quad \text{for all} \quad (x,y)\in\overline{\Omega}\times\mathbb{R}^{3\times3},$$

derived from the symmetry of the Cauchy-stress tensor. Finally it is assumed that

$$\frac{\partial a_{ij}}{\partial y_{hk}}(x,1)\sigma_{ij}\sigma_{hk}>0 \quad \text{for all} \quad x\in\overline{\Omega}.$$

Let $h : \Omega\to\mathbb{R}^3$ and $g : \partial\Omega\to\mathbb{R}^3$ be given functions. The pair (h,g) is equilibrated if

$$\int_\Omega h(x)dx+\int_{\partial\Omega} g(x)\,d\sigma = 0,$$

$$\int_\Omega (x_i\,h_j(x)-x_j\,h_i(x))\,dx+\int_{\partial\Omega}(x_i\,g_j(x)-x_j\,g_i(x))\,d\sigma=0 \quad i,j=1,\,2,\,3.$$

This implies the symmetry of the astatic tensor c of (h,g), defined by the relation

$$c_{ij}=\int_\Omega x_ih_j(x)\mathrm{d}x+\int_{\partial\Omega}x_ig_j(x)\mathrm{d}\sigma, \quad i,j=1,\,2,\,3.$$

Theorem Appendix A.1 (Lanza de Cristoforis and Valent) *Assume that Ω is a $\mathcal{C}^{m+2}$ domain, that $p(m+1)>3$, that a belongs to $(\mathcal{C}^{m+2}(\overline{\Omega}\times\mathbb{R}^{3\times3}))^{3\times3}$ and that the hypotheses (A.1) are satisfied. Let $(h,g)\in F_{m,p}$ be such that, if c_1, c_2, c_3 are the*

eigenvalues of the matrix c defined by (Appendix A.1), then $c_i + c_j \neq 0$ *when* $i \neq j$. *Then there exist two positive numbers* r *and* ρ *such that, if* $0 < |\lambda| \leq r$, *the problem (8) has one solution* $u \in (W^{m+2,p}(\Omega))^3$ *such that* $\int_\Omega u dx = 0$ *and* $\|u\|_{m+2,p} \leq \rho$.

Lemma Appendix A.1 *Assume* Ω *to be a* $\mathcal{C}^{m+2}$ *bounded domain,* $pm > 3$ *and that* $a \in (\mathcal{C}^{m+3}(\bar{\Omega} \times \mathbb{R}^{3\times 3}))^{3\times 3}$. *Then* L *is twice continuously differentiable, and bounded on a bounded ball :*

$$\sup_{\|u\|_{m+2,p} \leq \eta} \|L''(u)\| < \infty \quad \textit{for each} \quad \eta > 0.$$

The proof is given in [23].

Lemma Appendix A.2 (Lanza de Cristoforis and Valent) *Assume* Ω *to be a* $\mathcal{C}^{m+2}$ *bounded domain,* $(p+1)m > 3$ *and that* $a \in (\mathcal{C}^{m+2}(\bar{\Omega} \times \mathbb{R}^{3\times 3}))^{3\times 3}$ *such that hypotheses (A.1) apply. Then the operator* $L'(0)$ *is an isomorphism of* $V_{m,p}$ *onto* $F_{m,p}$.

Acknowledgments:
We thank Prof. M. Schatzman for interesting discussions and her constant support. We are very grateful to B. Hiba and M. Janier for providing the MR images of the mice. The Région Rhônes-Alpes is gratefully acknowledged for its help through the EURODOC project. This work is partially funded by ACI Masses de Donnes in the context of the AGIR project.

[1] Robert A. Adams. *Sobolev spaces*. Academic Press [A subsidiary of Harcourt Brace Jovanovich, Publishers], New York-London, 1975.

[2] T. Baker, P. Pebay, and J. Pousin. Dynamic meshing for finite element based segmentation of cardiac imagery. In *WCCM V - Fifth World Congress on Computational Mechanics*, Vienna, 2002.

[3] G. Borgefors. Distance transformation in digital images. *Computer Vision Graphics and Image Processing*, 48:344–371, 1986.

[4] Houman Borouchaki and Paul Louis George. Triangulation de Delaunay et métrique riemannienne. Applications aux maillages éléments finis. *Rev. Européenne Élém. Finis*, 5(3):323–340, 1996.

[5] Canny. A computational approach to edge detection. *IEEE Transactions on Pattern Analysis and Machine Intelligence*, 8:679–698, 1986.

[6] Vicent Caselles, Ron Kimmel, Guillermo Sapiro, and Catalina Sbert. Minimal surfaces: a geometric three-dimensional segmentation approach. *Numer. Math.*, 77(4):423–451, 1997.

[7] Philippe G. Ciarlet. *Mathematical elasticity. Vol. I*, volume 20 of *Studies in Mathematics and its Applications*. North-Holland Publishing Co., Amsterdam, 1988.

[8] Michel Crouzeix and Alain L. Mignot. *Analyse numérique des équations différentielles*. Collection Mathématiques Appliquées pour la Maîtrise. Masson, Paris, 1984.

[9] M. Lanza De Cristoforis and T. Valent. On Neumann's problem for a quasilinear differential system of the finite elastostatics type. Local theorems of existence and uniqueness. *Rend. Sem. Mat. Univ. Padova*, 68:183–206 (1983), 1982.

[10] J. Droux. *Simulation numérique bidimensionnelle de processus de solidification*. PhD thesis, EPFL, 1990.

[11] A. F. Frangi, W. J. Niessen, and M. A. Viergever. Three-dimensional modeling for functional analysis of cardiac images, a review. *IEEE Transactions on Medical Imaging*, 20(1):2–25, 2001.

[12] Gary Jacob, Alison J. Noble, Miguel Mulet-Parada, and Andrew Blake. Evaluating a robust contour tracker on echocardiographic sequences. *Medical Image Analysis*, 3(1):63–75, 1999.

[13] Michael R. Kaus, Jens von Berg, Jürgen Weese, Wiro Niessen, and Vladimir Pekar. Automated segmentation of the left ventricle in cardiac MRI. *Medical Image Analysis*, 8:245–254, 2004.

[14] Gregory. J. Klein and Ronald H. Huesman. Four-dimensional processing of deformable cardiac PET data. *Medical Image Analysis*, 6:29–46, 2002.

[15] Maria Lorenzo-Valdés, Gerardo I. Sanchez-Ortiz, Andrew G. Elkington, Raad H. Mohiaddin, and Daniel Rueckert. Segmentation of 4D cardiac MR images using a probabilistic atlas and the EM algorithm. *Medical Image Analysis*, 8:255–265, 2004.

[16] Jyrki Lötjönen, S. Kivistö, J. Koikkalainen, D. Smutek, and Kirsi Lauerma. Statistical shape model of atria, ventricles and epicardium from short- and long-axis MR images. *Medical Image Analysis*, 8:371–386, 2004.

[17] T. Mäkelä, Quoc Cuong Pham, P. Clarysse, J. Nenonen, J. Lötjönen, O. Sipilä, H. Hänninen, K. Lauerma, J. Knutti, T. Katila, and I.E. Magnin. A 3d model-based registration approach for the pet, mr and mcg cardiac data fusion. *Medical Image Analysis*, 7(3):377–389, 2003.

[18] Steven C. Mitchell, Johan G. Bosch, Boudewijn P. F. Lelieveldt, Rob J. van der Geest, J. H. C. Reiber, and Milan Sonka. 3D active appearance models: segmentation of cardiac MR and ultrasound images. *IEEE Transactions on Medical Imaging*, 21(9):1167–1178, 2002.

[19] J. Montagnat and H. Delingette. A review of deformable surfaces: topology, geometry and deformation. *Image and Vision Computing*, 19(14):1023–1040, 2001.

[20] Stanley Osher and James A. Sethian. Fronts propagating with curvature-dependent speed: algorithms based on hamilton-jacobi formulations. *J. Comput. Phys.*, 79(1):12–49, 1988.

[21] Q.-C. Pham, F. Vincent, P. Clarysse, P. Croisille, and I. E. Magnin. A FEM-based deformable model for the 3D segmentation and tracking of the heart in cardiac MRI. In *2nd International Symposium on Image and Signal Processing and Analysis (ISPA 2001)*, volume 1, pages 250–254, Pula, Croatia, 2001.

[22] Q.C. Pham. *Segmentation et mise en correspondance en imagerie cardiaque multimodale conduites par un modèle anatomique bi-cavités du coeur*. PhD thesis, INPG, 2002.

[23] Y. Rouchdy, J. Pousin, J. Schaerer, and P. Clarysse. A nonlinear elastic deformable template for soft structure segmentation. Application to the heart segmentation in MRI. *Accepted in Inverse Problems (minor revision)*, 2007.

[24] T. Saito and T.I. Toriwaki. New algorithm for euclidean distance transformation of an n-dimensional digitized picture with applications. *Pattern recognition*, 27:1551–1565, 1994.

[25] J Schaerer, Y Rouchdy, P Clarysse, B Hiba, P Croisille, J Pousin, and IE Magnin. Simultaneous segmentation of the left and right heart ventricles in 3D cine MR images of small animals. In *Proceedings of Computers in Cardiology*, pages 231–234, Lyon, 2005.

[26] C. Xu and J.L. Prince. Snakes, shapes, and gradient vector flow. *IEEE Trans. Image Processing*, 7:359–369, 1998.